

## LETTERS

# 53BP1 promotes non-homologous end joining of telomeres by increasing chromatin mobility

Nadya Dimitrova<sup>1</sup>, Yi-Chun M. Chen<sup>2</sup>, David L. Spector<sup>2</sup> & Titia de Lange<sup>1</sup>

Double-strand breaks activate the ataxia telangiectasia mutated (ATM) kinase, which promotes the accumulation of DNA damage factors in the chromatin surrounding the break. The functional significance of the resulting DNA damage foci is poorly understood. Here we show that 53BP1 (also known as TRP53BP1), a component of DNA damage foci, changes the dynamic behaviour of chromatin to promote DNA repair. We used conditional deletion of the shelterin component TRF2 (also known as TEF2) from mouse cells (*TRF2*<sup>fl/-</sup>) to deprotect telomeres, which, like double-strand breaks, activate the ATM kinase, accumulate 53BP1 and are processed by non-homologous end joining (NHEJ)<sup>1,2</sup>. Deletion of TRF2 from 53BP1-deficient cells established that NHEJ of dysfunctional telomeres is strongly dependent on the binding of 53BP1 to damaged chromosome ends. To address the mechanism by which 53BP1 promotes NHEJ, we used time-lapse microscopy to measure telomere dynamics before and after their deprotection. Imaging showed that deprotected telomeres are more mobile and sample larger territories within the nucleus. This change in chromatin dynamics was dependent on 53BP1 and ATM but did not require a functional NHEJ pathway. We propose that the binding of 53BP1 near DNA breaks changes the dynamic behaviour of the local chromatin, thereby facilitating NHEJ repair reactions that involve distant sites, including joining of dysfunctional telomeres and AID (also known as AICDA)-induced breaks in immunoglobulin class-switch recombination.

Previous work has shown that mouse telomeres lacking TRF2 are processed by a KU70- and DNA-ligase-IV-dependent NHEJ reaction<sup>1,2</sup> that requires ATM kinase signalling and is stimulated by the ATM targets H2AX (also known as H2AFX) and MDC1 (refs 3 and 4). Here we focus on 53BP1, a third ATM target, which accumulates at double-strand breaks (DSBs) and deprotected telomeres<sup>5-8</sup>. The interaction of 53BP1 with chromatin involves the binding of its tudor domains to H4K20me2 and an MDC1-dependent interaction with  $\gamma$ -H2AX<sup>9-14</sup>. Although 53BP1 is not strictly required for DNA damage signalling, homology-directed repair or NHEJ in the context of V(D)J recombination, NHEJ of DSBs in class-switch recombination (CSR) is severely affected by 53BP1 deficiency<sup>15,16</sup>. In the absence of 53BP1, DSBs in different switch regions fail to join successfully, resulting in a predominance of intra-switch recombination events<sup>17</sup>. It has been proposed that 53BP1 might either facilitate synapsis of DNA ends<sup>17,18</sup> or 'shepherd' NHEJ factors to the break<sup>19</sup>.

We generated SV40LT immortalized *TRF2*<sup>fl/-</sup>*53BP1*<sup>-/-</sup> and *TRF2*<sup>fl/-</sup>*53BP1*<sup>+/-</sup> mouse embryonic fibroblasts (MEFs)<sup>1,20</sup> (Supplementary Fig. 1a, b) and assayed the frequency of telomere fusions in metaphase spreads collected 120 h after Cre-mediated deletion of TRF2 (Fig. 1a). Whereas 53BP1-proficient cells showed the expected level of telomere fusions (33% of telomeres fused after four population doublings), the rate of NHEJ in *53BP1*<sup>-/-</sup> cells was at least 50-fold lower, nearly as low as that in DNA-ligase-IV-defi-

cient cells<sup>1,2</sup>. The effect of 53BP1 on telomere fusions was also obvious when assayed by an in-gel hybridization assay (Fig. 1b). Cells deficient for 53BP1 failed to accumulate high-molecular-weight fusion products after deletion of TRF2 and showed no loss of the telomeric 3' overhang, a second index for telomere fusion (Fig. 1b, c). In fact, the overhang signal increased, similar to what is observed when TRF2 is deleted from KU70- or DNA-ligase-IV-deficient cells<sup>1,2</sup>. In contrast to NHEJ, DNA damage signalling was not affected by the absence of 53BP1 (Fig. 1d, e). Deficiency of 53BP1 affected neither the phosphorylation of ATM and its target CHK2 (also known as CHEK2) nor the presence of  $\gamma$ -H2AX, MDC1 and NBS1 (also known as NBN) at dysfunctional telomeres (Fig. 1d, e and Supplementary Fig. 2a, b). The NHEJ defect was also not due to a change in cell cycle progression. After deletion of TRF2, the cells underwent the same number of cell divisions regardless of their 53BP1 status (Fig. 1f), and their S-phase index was not affected by 53BP1 deficiency (Supplementary Fig. 1c).

We next tested whether the tudor-domain-mediated recognition of H4K20me2 contributed to the promotion of NHEJ. *TRF2*<sup>fl/-</sup>*53BP1*<sup>-/-</sup> cells were complemented with wild-type human 53BP1 or with a tudor domain mutant (53BP1(D1521A)) with impaired binding to H4K20me2 (ref. 14; Fig. 2a). Although the two forms of 53BP1 were expressed at levels comparable to endogenous 53BP1 (Fig. 2b and data not shown), the recruitment of 53BP1(D1521A) to deprotected telomeres was diminished (Supplementary Fig. 3). In contrast to wild-type 53BP1, which reconstituted the NHEJ of dysfunctional telomeres, cells expressing the tudor mutant of 53BP1 showed a considerable delay in the fusion of telomeres lacking TRF2 (Fig. 2c, d).

The finding that the tudor domain mutation in 53BP1 did not abrogate NHEJ suggested that a second, H4K20me2-independent, interaction of 53BP1 with chromatin contributes to NHEJ. Because MDC1 is required for the stable association of 53BP1 with DSBs<sup>9-14</sup>, we generated *TRF2*<sup>fl/fl</sup>*Mdc1*<sup>-/-</sup> MEFs<sup>18</sup> and determined their ability to execute the telomere fusion reaction. As expected, the binding of 53BP1 near deprotected telomeres was impaired by MDC1 deficiency, despite normal levels of H2AX phosphorylation (Supplementary Fig. 4a, b). MDC1 deficiency resulted in a delay in the NHEJ of telomeres but did not abrogate this process (Supplementary Fig. 5a, b), confirming our previous findings with MDC1 short hairpin RNAs (shRNAs)<sup>3</sup>. Furthermore, inhibition of MDC1 with shRNAs affected the residual NHEJ of telomeres in the context of the 53BP1 tudor domain mutant (Supplementary Fig. 5c-e).

These data establish an important role for chromatin-bound 53BP1 in the NHEJ of deprotected telomeres. Previous data showed that 53BP1 contributes to NHEJ in CSR<sup>15,16</sup>, but not in other settings such as V(D)J recombination. We argued that the crucial difference between the 53BP1-dependent and-independent NHEJ reactions

<sup>1</sup>The Rockefeller University, 1230 York Avenue, New York, New York 10065, USA. <sup>2</sup>Cold Spring Harbor Laboratory, One Bungtown Road, Cold Spring Harbor, New York 11724, USA.

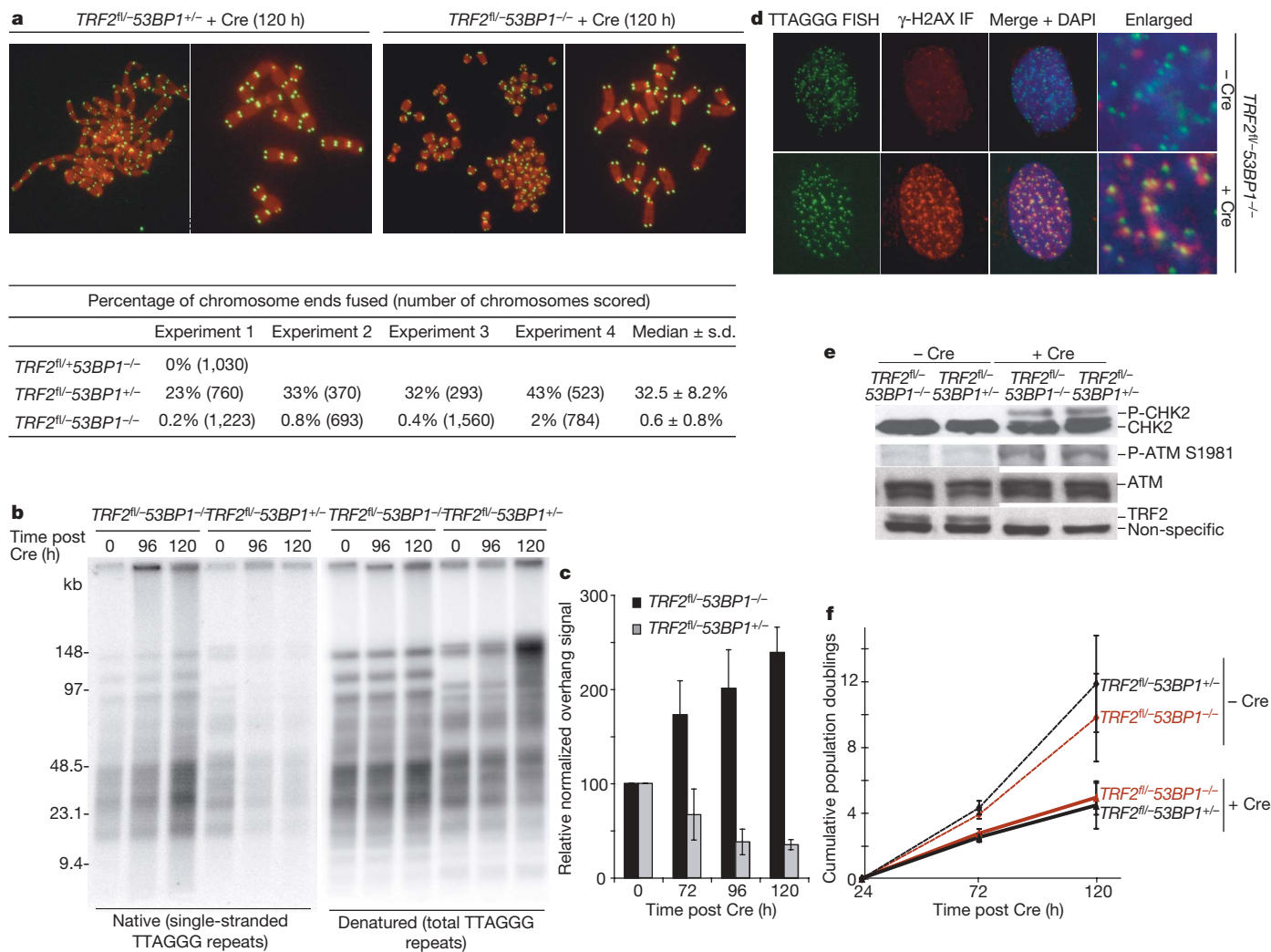


**Figure 1 | Requirement for 53BP1 in NHEJ of dysfunctional telomeres, but not in DNA damage signalling.** **a**, Metaphase chromosomes after deletion of TRF2 from the indicated cells (top). Telomeric fluorescence *in situ* hybridization (FISH), green; 4,6-diamidino-2-phenylindole (DAPI), red. Summary of the effect of 53BP1 on telomere fusions 120 h after TRF2 deletion (bottom). **b**, In-gel assay for the 3' overhang (left) and total telomeric DNA (right) after deletion of TRF2 from 53BP1-proficient

and -deficient cells. **c**, Quantification of overhang signals in **b** (mean  $\pm$  s.d.;  $n = 3$ ). **d**, Immunofluorescence (IF) for the presence of  $\gamma$ -H2AX at telomeres after deletion of TRF2 from 53BP1-proficient and -deficient cells.

**e**, Immunoblots for phosphorylated (P-) ATM and CHK2 after TRF2 deletion. **f**, Proliferation of MEFs of the indicated genotype and treatment (mean  $\pm$  s.d.;  $n = 3$ ).

might be the distance between the DNA ends involved. Whereas the two ends generated by RAG1/2 or chromosome-internal DNA damage are close together, the DNA ends generated by AID in CSR are often far apart, as are dysfunctional telomeres in G1 when they are processed by NHEJ (ref. 21).

We used time-lapse microscopy to address whether 53BP1 altered the synapsis and/or dynamics of deprotected telomeres. To image telomeres, we used enhanced-green-fluorescent-protein-tagged version of the shelterin component TRF1 (eGFP-TRF1), which remains associated with telomeres when TRF2 is removed (Fig. 3a-c and Supplementary Fig. 6). Overexpression of this and other forms of TRF1 does not affect the protective function of telomeres<sup>22</sup> (data not shown). To mark sites of DNA damage signalling, we fused mCherry to amino acids 1220-1711 of 53BP1 (mCherry-BP1-2, see Figs 2a and 3a, b), creating a fusion protein that lacks most of the functional domains of 53BP1. On deletion of TRF2, mCherry-BP1-2 re-localized to telomeric sites containing eGFP-TRF1 (Fig. 3c). The mCherry-BP1-2 allele did not affect the frequency of telomere fusions in 53BP1-proficient cells nor did it restore the NHEJ defect in 53BP1-deficient cells (Supplementary Fig. 7a), establishing that it is a neutral marker for DNA damage in this context. Furthermore,

imaging experiments repeated in cells lacking mCherry-BP1-2 gave the same outcome (Supplementary Fig. 7b, c and see below).

To analyse the effect of 53BP1 on the movement of dysfunctional telomeres, time-lapse microscopy was performed at an early stage after deletion of TRF2 (72-84 h post-Cre) when most TRF1-marked sites still represent free chromosome ends<sup>3</sup>. Initial analysis of eGFP and mCherry signals indicated that dysfunctional telomeres became more mobile but only when 53BP1 was present (Supplementary Videos 1 and 2). We observed occasional apparent fusion events in 53BP1-proficient cells (Supplementary Video 3), but no potential fusions were observed in 53BP1-deficient cells, even for telomeres that were closely apposed (Supplementary Video 4).

To obtain a quantitative measure of telomere mobility, individual eGFP-TRF1/mCherry-BP1-2-labelled dysfunctional telomeres were traced in deconvolved and projected images (Fig. 3a, d and Supplementary Fig. 8a, b). In parallel, eGFP-TRF1-marked functional telomeres were analysed in cells not treated with Cre. Functional telomeres in 53BP1-proficient and -deficient cells travelled in a constrained random walk over a total path of approximately 3.7-3.9  $\pm$  0.7  $\mu$ m at a median speed of 180-190 nm min<sup>-1</sup>, which is comparable to the movement of human telomeres (Fig. 3e, f and

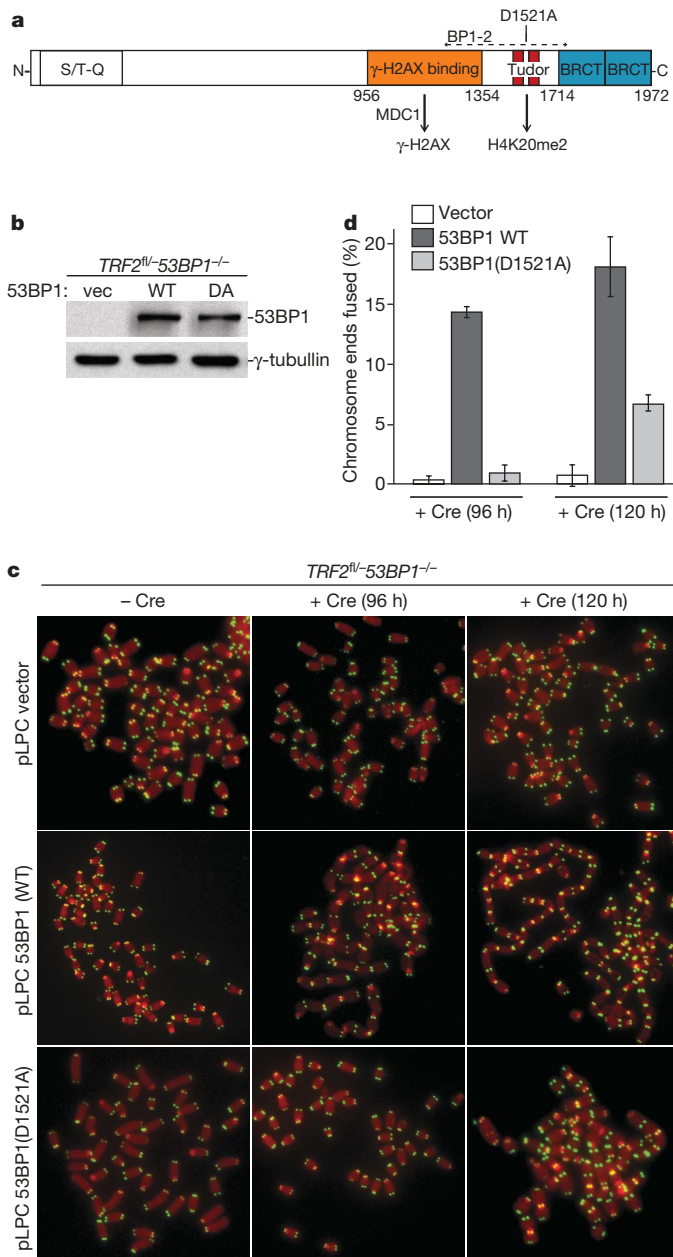


**Figure 2 | Optimal NHEJ of dysfunctional telomeres requires interaction of 53BP1 with H4K20me2.** **a**, Schematic of the domain structure of 53BP1 highlighting the N-terminal cluster of S/T-Q phosphorylation sites, the tudor domain and BRCT (BRCA1 C-terminal) repeats. **b**, Immunoblot for 53BP1 expression in *TRF2<sup>fl/fl</sup>-53BP1<sup>-/-</sup>* cells complemented with empty vector (vec), wild type (WT) or the tudor mutant 53BP1(D1521A) (DA). **c**, Telomere fusions in metaphase spreads of *TRF2<sup>fl/fl</sup>-53BP1<sup>-/-</sup>* MEFs complemented as indicated and treated with Cre as specified. **d**, Quantification of telomere fusions in **c** (mean  $\pm$  s.d.;  $n = 3$ ).

Supplementary Figs 7b and 9a)<sup>23</sup>. In contrast, dysfunctional telomeres were significantly more mobile, travelling at a speed of 270–360 nm min<sup>-1</sup> over a cumulative distance ranging from 5.4  $\mu$ m to 7.2  $\mu$ m (Fig. 3e, f and Supplementary Figs 7b and 9a). The mobility increase associated with telomere dysfunction was significantly attenuated in cells lacking 53BP1 (Fig. 3e), resulting in a median cumulative distance travelled of 4.4  $\pm$  0.2  $\mu$ m. The presence of the mCherry-BP1-2 DNA damage marker did not affect the outcome; the same results were obtained after deletion of TRF2 from *53BP1<sup>+/-</sup>* or *53BP1<sup>-/-</sup>* cells that only contained the eGFP-TRF1 marker (Supplementary Fig. 7b, c). Importantly, in both settings the dysfunctional telomeres in 53BP1-proficient cells sampled larger

territories than functional telomeres (maximal displacement 1.2  $\pm$  0.3  $\mu$ m versus 0.51  $\pm$  0.29  $\mu$ m; Fig. 3g and Supplementary Figs 7c and 9b). Assuming that telomeres sample spheres within the nucleus, a twofold change in the radius of the two-dimensional territory will increase the volume sampled by a dysfunctional telomere by a factor of eight. Furthermore, a substantial fraction (>10%) of the dysfunctional telomeres roamed well beyond 2  $\mu$ m, whereas none of the 115 functional telomeres analysed moved beyond that distance (Fig. 3g and Supplementary Fig. 7c). When 53BP1 was not present, the median maximal displacement of the dysfunctional telomeres was only 0.8  $\pm$  0.2  $\mu$ m, indicating movement within a significantly smaller territory, and only one out of 115 dysfunctional telomeres sampled an area beyond 2  $\mu$ m (Fig. 3g and Supplementary Fig. 7c). These data establish that telomeres become more mobile and sample larger territories when they are deprived of their normal protection and that this change in their dynamic behaviour is promoted by 53BP1. Assuming that the rate of NHEJ correlates with the probability of an encounter between two telomeres, the ability of 53BP1 to expand the three-dimensional space visited by dysfunctional telomeres is a probable explanation for its effect on telomere fusion. We confirmed that the absence of the NHEJ reaction itself could not account for the slower movement because telomeres in DNA-ligase-IV-deficient cells still showed a considerable increase in their mobility on TRF2 deletion (Fig. 3h and Supplementary Fig. 9c, d).

The ability of 53BP1 to promote the mobility of dysfunctional telomeres could explain why ATM kinase, its upstream regulator, is required for telomere fusions<sup>4</sup>. Indeed, similar to 53BP1-deficient cells, dysfunctional telomeres failed to gain their maximal mobility in ATM-deficient cells (Fig. 3i and Supplementary Fig. 9c, d).

Next we tested whether 53BP1 caused global chromatin mobility in response to DNA damage. We tracked functional telomeres in wild-type or *Lig4<sup>-/-</sup>* cells immediately after treatment with  $\gamma$ -irradiation or after allowing the cells to recover. In all cases, we found that the mobility of the telomeres was unaffected by the induction of damage elsewhere in the genome (Supplementary Fig. 10), arguing that increased mobility is a local event, taking place at the site of damage where 53BP1 accumulates.

Because 53BP1 is the first DNA damage factor to be implicated in the movement of sites of DNA damage, it will be important to determine the mechanism by which it affects chromatin mobility. Latrunculin A did not alter the gain in mobility of deprotected telomeres (Supplementary Fig. 11a), arguing against an actin-driven process. Similarly, the histone deacetylase (HDAC) inhibitor trichostatin A had no effect on the mobility of the deprotected telomeres, making it unlikely that 53BP1 acts through its interaction with HDAC4 (ref. 24; Supplementary Fig. 11b). We imagine that 53BP1 dislodges a factor that restricts chromatin mobility or that 53BP1 endows the chromatin with dynamic features, for instance by altering higher order interactions that affect the length of thermal persistence.

These data reveal that the DNA damage factor 53BP1 is crucial for the NHEJ reaction at dysfunctional telomeres and suggest a mechanism by which 53BP1 promotes telomere fusions. Telomeres, like other chromosomal sites, have a limited range of motion, showing constrained diffusion within a territory with a radius of  $\leq$ 0.5  $\mu$ m (this work and refs 23 and 25). When telomeres become damaged, their mobility increases significantly, which is expected to increase the chance that two dysfunctional telomeres become closely apposed, thereby allowing the NHEJ machinery to engage the two DNA ends. Given that 53BP1 is also important for CSR, we suggest that the change in chromatin dynamics also promotes the joining of AID-induced breaks. In an accompanying paper<sup>26</sup>, this paradigm is further extended to distant DSBs in V(D)J recombination. We therefore suggest that 53BP1 is a facilitator of NHEJ at all distant DNA ends, acting by increasing the mobility of the local chromatin. Because joining of distant DNA ends promotes chromosome rearrangements, we consider it unlikely that the main role of 53BP1 is to promote

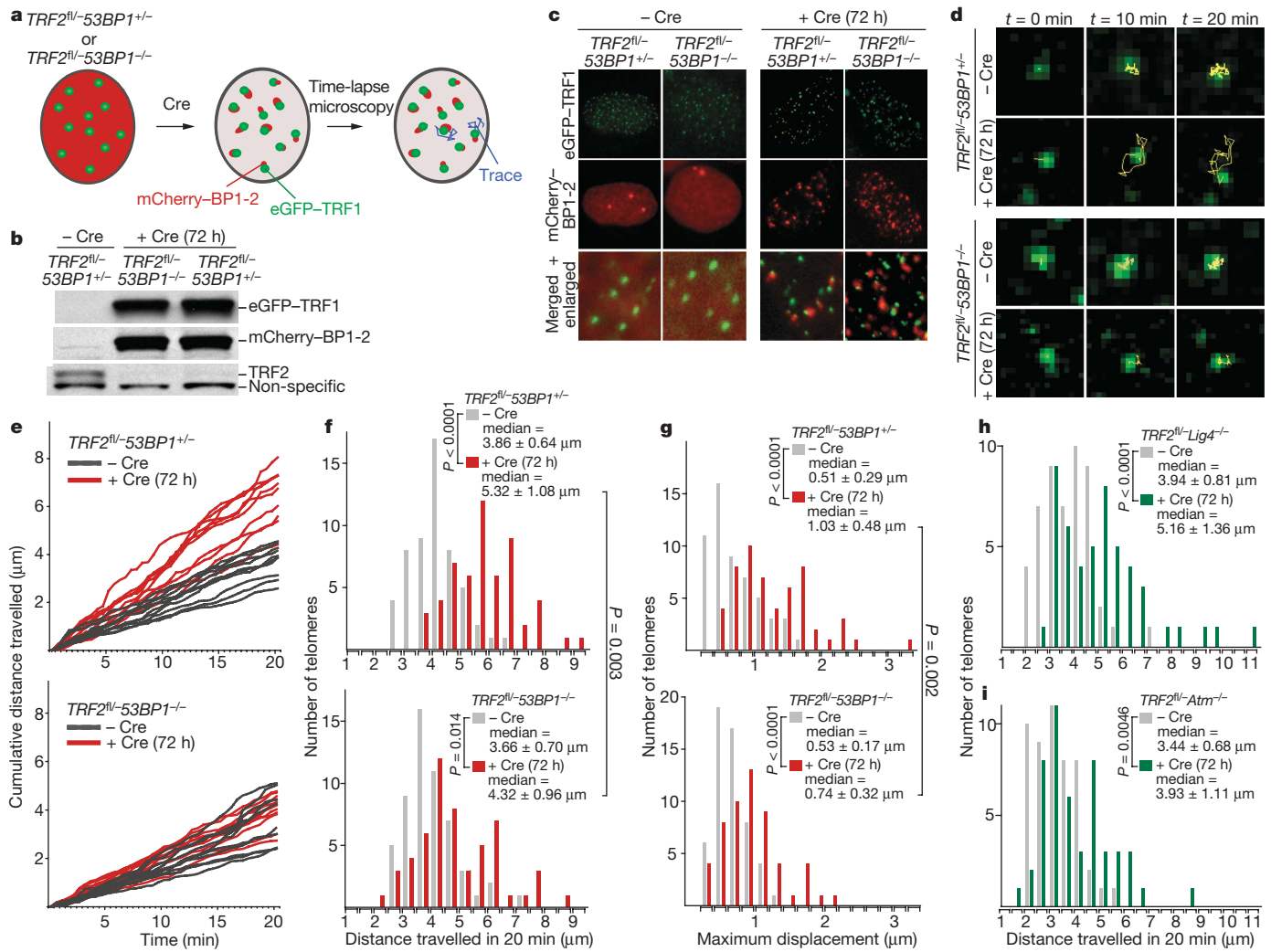


**Figure 3** | 53BP1 promotes mobility of dysfunctional telomeres.

**a**, Schematic of the live-cell imaging experiments. **b**, Immunoblotting for eGFP-TRF1, mCherry-BP1-2 and TRF2. **c**, Co-localization of eGFP-TRF1 and mCherry-BP1-2 fluorescence signals. **d**, Representative traces of telomeres in indicated MEFs expressing eGFP-TRF1 and mCherry-BP1-2. Snapshots taken at indicated time points. **e**, Ten representative telomeres from indicated MEFs, treated as specified, were tracked as in **d**; the cumulative distance at each time point is plotted against time. **f**, Frequency

distribution of the cumulative distance travelled in one representative experiment in MEFs of the indicated genotype and treatment (median  $\pm$  s.d.;  $n = 55$ ;  $P$  was calculated using a two-tailed Mann-Whitney test). **g**, Frequency distribution of the maximum displacement from the starting point registered by individual telomeres during the imaging session described in **f** (median  $\pm$  s.d. and  $P$  values were calculated as in **f**). **h**, **i**, Analysis as in **f** in MEFs of the indicated genotypes and treatments, expressing the eGFP-TRF1 marker only ( $n = 50$ ).

NHEJ at DNA ends that are far apart. It seems more likely that the increased chromatin mobility we observe reflects an attribute of 53BP1-containing chromatin that is important for DNA repair at all DSBs, including those that are closely apposed and breaks that are processed by homology-directed repair. We imagine that at telomeres this chromatin change leads to increased mobility, whereas at chromosome-internal DSBs the same change in the chromatin may facilitate their repair in other ways.

## METHODS SUMMARY

MEFs from embryonic day (E)13.5 embryos obtained from crosses between *TRF2<sup>fl/-</sup>* and *53BP1<sup>+/-</sup>* mice<sup>1,20</sup> were isolated and immortalized at passage 2 with pBabeSV40LT (a gift from G. Hannon). Cre was introduced by retroviral infection with pMMP Hit&Run Cre<sup>27</sup>. For time-lapse microscopy, *TRF2<sup>fl/-</sup>53BP1<sup>+/-</sup>* and *TRF2<sup>fl/-</sup>53BP1<sup>-/-</sup>* cells expressing eGFP-TRF1 and mCherry-BP1-2, or *TRF2<sup>fl/-</sup>Lig4<sup>+/-</sup>p53<sup>-/-</sup>* (ref. 1) and *TRF2<sup>fl/-</sup>Atr<sup>-/-</sup>* (ref. 4) cells expressing eGFP-TRF1 only, were imaged untreated or 72 h after Cre-mediated deletion of TRF2. Time-lapse images were acquired using a DeltaVision RT microscope system (Applied Precision) in three dimensions in both eGFP and mCherry channels using SoftWoRx software every 30 s for 20 min. Images were deconvolved, projected in two dimensions, and tracking analysis was performed with ImageJ. Data were collected from three independent

experiments ( $n \geq 50$ ) and Mann-Whitney statistical analysis was performed using Prism software.

**Full Methods** and any associated references are available in the online version of the paper at [www.nature.com/nature](http://www.nature.com/nature).

Received 19 April; accepted 19 September 2008.  
Published online 19 October 2008.

1. Celli, G. & de Lange, T. DNA processing not required for ATM-mediated telomere damage response after TRF2 deletion. *Nature Cell Biol.* **7**, 712–718 (2005).
2. Celli, G. B., Lazzarini Denchi, E. & de Lange, T. Ku70 stimulates fusion of dysfunctional telomeres yet protects chromosome ends from homologous recombination. *Nature Cell Biol.* **8**, 855–890 (2006).
3. Dimitrova, N. & de Lange, T. MDC1 accelerates non-homologous end-joining of dysfunctional telomeres. *Genes Dev.* **20**, 3238–3243 (2006).
4. Lazzarini Denchi, E. & de Lange, T. Protection of telomeres through independent control of ATM and ATR by TRF2 and POT1. *Nature* **448**, 1068–1071 (2007).
5. DiTullio, R. A. Jr *et al.* 53BP1 functions in an ATM-dependent checkpoint pathway that is constitutively activated in human cancer. *Nature Cell Biol.* **4**, 998–1002 (2002).
6. Wang, B., Matsuoka, S., Carpenter, P. B. & Elledge, S. J. 53BP1, a mediator of the DNA damage checkpoint. *Science* **298**, 1435–1438 (2002).
7. Fernandez-Capetillo, O., Liebe, B., Scherthan, H. & Nussenzweig, A. H2AX regulates meiotic telomere clustering. *J. Cell Biol.* **163**, 15–20 (2003).

8. Takai, H., Smogorzewska, A. & de Lange, T. DNA damage foci at dysfunctional telomeres. *Curr. Biol.* **13**, 1549–1556 (2003).
9. Goldberg, M. *et al.* MDC1 is required for the intra-S-phase DNA damage checkpoint. *Nature* **421**, 952–956 (2003).
10. Lou, Z., Minter-Dykhouse, K., Wu, X. & Chen, J. MDC1 is coupled to activated CHK2 in mammalian DNA damage response pathways. *Nature* **421**, 957–961 (2003).
11. Stewart, G. S., Wang, B., Bignell, C. R., Taylor, A. M. & Elledge, S. J. MDC1 is a mediator of the mammalian DNA damage checkpoint. *Nature* **421**, 961–966 (2003).
12. Ward, I. M., Minn, K., Jorda, K. G. & Chen, J. Accumulation of checkpoint protein 53BP1 at DNA breaks involves its binding to phosphorylated histone H2AX. *J. Biol. Chem.* **278**, 19579–19582 (2003).
13. Bekker-Jensen, S., Lukas, C., Melander, F., Bartek, J. & Lukas, J. Dynamic assembly and sustained retention of 53BP1 at the sites of DNA damage are controlled by Mdc1/NFBD1. *J. Cell Biol.* **170**, 201–211 (2005).
14. Botuyan, M. V. *et al.* Structural basis for the methylation state-specific recognition of histone H4–K20 by 53BP1 and Crb2 in DNA repair. *Cell* **127**, 1361–1373 (2006).
15. Manis, J. P. *et al.* 53BP1 links DNA damage-response pathways to immunoglobulin heavy chain class-switch recombination. *Nature Immunol.* **5**, 481–487 (2004).
16. Ward, I. M. *et al.* 53BP1 is required for class switch recombination. *J. Cell Biol.* **165**, 459–464 (2004).
17. Reina-San-Martin, B., Chen, J., Nussenzweig, A. & Nussenzweig, M. C. Enhanced intra-switch region recombination during immunoglobulin class switch recombination in 53BP1<sup>-/-</sup> B cells. *Eur. J. Immunol.* **37**, 235–239 (2007).
18. Lou, Z. *et al.* MDC1 maintains genomic stability by participating in the amplification of ATM-dependent DNA damage signals. *Mol. Cell* **21**, 187–200 (2006).
19. Xie, A. *et al.* Distinct roles of chromatin-associated proteins MDC1 and 53BP1 in mammalian double-strand break repair. *Mol. Cell* **28**, 1045–1057 (2007).
20. Ward, I. M., Minn, K., van Deursen, J. & Chen, J. p53 binding protein 53BP1 is required for DNA damage responses and tumor suppression in mice. *Mol. Cell Biol.* **23**, 2556–2563 (2003).
21. Konishi, A. & de Lange, T. Cell cycle control of telomere protection and NHEJ revealed by a ts mutation in the DNA-binding domain of TRF2. *Genes Dev.* **22**, 1221–1230 (2008).
22. van Steensel, B. & de Lange, T. Control of telomere length by the human telomeric protein TRF1. *Nature* **385**, 740–743 (1997).
23. Molenaar, C. *et al.* Visualizing telomere dynamics in living mammalian cells using PNA probes. *EMBO J.* **22**, 6631–6641 (2003).
24. Kao, G. D. *et al.* Histone deacetylase 4 interacts with 53BP1 to mediate the DNA damage response. *J. Cell Biol.* **160**, 1017–1027 (2003).
25. Abney, J. R., Cutler, B., Fillbach, M. L., Axelrod, D. & Scalettar, B. A. Chromatin dynamics in interphase nuclei and its implications for nuclear structure. *J. Cell Biol.* **137**, 1459–1468 (1997).
26. Difilippantonio, S. *et al.* 53BP1 Facilitates long-range DNA end-joining during V(D)J recombination. *Nature* doi:10.1038/nature07476 (this issue).
27. Silver, D. P. & Livingston, D. M. Self-excising retroviral vectors encoding the Cre recombinase overcome Cre-mediated cellular toxicity. *Mol. Cell* **8**, 233–243 (2001).

**Supplementary Information** is linked to the online version of the paper at [www.nature.com/nature](http://www.nature.com/nature).

**Acknowledgements** We are grateful to J. Chen for his gift of 53BP1- and MDC1-deficient mice. We thank D. White for expert mouse husbandry. We thank the Bio-Imaging Facilities at Cold Spring Harbor Laboratory and at The Rockefeller University. J. Petrini is thanked for his gift of NBS1 antibody, A. Sfeir for providing the TRF1 antibody and A. Konishi for the BP1-2 construct. M. Dimitrov is thanked for mathematical advice on data analysis, and S. Jaramillo and Y. Fu for Matlab programming. Members of the de Lange laboratory are thanked for comments on the manuscript. This work was supported by a grant from the NIH (GM049046) and by the NIH Director's Pioneer Award (OD000379) to T.d.L., and grants from the NIH to D.L.S. (EY18244 and GM42694). N.D. was supported by an HHMI pre-doctoral fellowship.

**Author Contributions** N.D. and T.d.L. planned and designed the experiments. N.D. performed all experiments. Y.-C.M.C. and D.L.S. provided assistance with the imaging experiments. N.D. and T.d.L. wrote the paper and made the figures.

**Author Information** Reprints and permissions information is available at [www.nature.com/reprints](http://www.nature.com/reprints). Correspondence and requests for materials should be addressed to T.d.L. ([delange@mail.rockefeller.edu](mailto:delange@mail.rockefeller.edu)).

## METHODS

**Generation of MEFs and deletion of TRF2.** MEFs from E13.5 embryos obtained from crosses between *TRF2<sup>fl/fl</sup>* and *53BP1<sup>+/-</sup>* mice<sup>1,20</sup> and between *TRF2<sup>fl/fl</sup>* and *Mdc1<sup>+/-</sup>* mice<sup>18</sup> were isolated and immortalized at passage 2 with pBabeSV40LT. To delete TRF2, Cre was introduced by retroviral infection using the pMMP Hit&Run Cre retroviral construct<sup>27</sup>. In brief, Hit&Run Cre was expressed in ecotrophic Phoenix cells. Virus-containing supernatant was collected at 36, 48 and 60 h post-transfection and MEFs were infected consecutively three times every 12 h. The medium was changed 12 h after the last infection, and cells were analysed at the indicated time points after the second infection.

**Constructs.** Full-length human 53BP1 was cloned by PCR into a N-Myc-pLPC-puro retroviral expression vector. The D1521A mutation was introduced by a PCR-based mutagenesis strategy using the following mutagenesis primers: 5'-AAATGCTCTTTGATGCTGGGTACGAATGTGAT-3' and 5'-ATCACATTCGTACCCAGCATCAAAGAGCAATTT-3'. The mutation was confirmed by sequencing. Wild-type and D1521A rescue alleles were introduced into *TRF2<sup>fl/fl</sup>*-*53BP1<sup>-/-</sup>* cells by five consecutive retroviral infections, delivered at 12-h intervals with virus-containing supernatants from Phoenix cells. Puromycin selection was applied. Infection with the empty vector was used as a negative control.

Fluorescently amino-terminally tagged mCherry-BP1-2 and eGFP-TRF1 were cloned by PCR into pLPC-puro and pWz1-hygro, respectively. In-frame fusions were confirmed by sequencing. mCherry-BP1-2 and eGFP-TRF1 constructs were consecutively introduced into *TRF2<sup>fl/fl</sup>*-*53BP1<sup>+/-</sup>* and *TRF2<sup>fl/fl</sup>*-*53BP1<sup>-/-</sup>* cells by retroviral infections, followed by puromycin (4 days) and hygromycin (7 days) selection, respectively.

**MDC1 shRNAs.** MDC1 was stably reduced in *TRF2<sup>fl/fl</sup>*-*53BP1<sup>-/-</sup>* cells expressing the 53BP1(D1521A) mutant using shRNAs expressed from the pSUPERIOR retroviral vector (OligoEngine). Retrovirus was produced in ecotrophic Phoenix cells and used to infect cells four times at 12-h intervals. No selection was applied. The following target sequences<sup>3</sup> were cloned into pSUPERIOR and confirmed by DNA sequencing: mouse *Mdc1* sh4, 5'-ACAGCATGCAGTAATTGAA-3'; mouse *Mdc1* sh5, 5'-ACACAGCCGTTCTGTCTAA-3'. Infections with the empty vector were used as a negative control. Efficient knockdown of *Mdc1* was verified by immunoblotting.

**Telomere fluorescence *in situ* hybridization.** Cells were collected at the indicated time points after Cre infection and fixed as described previously<sup>28</sup>. Metaphase spreads were aged overnight and peptide nucleic acid (PNA) FISH<sup>29</sup> was performed. In brief, slides were washed in PBS once and fixed in 4% formaldehyde for 2 min at room temperature (24–25 °C). After extensive PBS washes, spreads were digested for 10 min at 37 °C with 1 mg ml<sup>-1</sup> pepsin dissolved in 10 mM glycine, pH 2.2. Slides were then washed in PBS, fixed again in 4% formaldehyde for 2 min at room temperature, and washed in PBS before dehydration by consecutive 5-min incubations in 70%, 95% and 100% ethanol. After air-drying, Hybridizing Solution (70% formamide, 1 mg ml<sup>-1</sup> blocking reagent (Roche), 10 mM Tris-HCl, pH 7.2) containing Flu-OO-(AATCCC)<sub>3</sub> PNA probe (Applied Biosystems) was added and spreads were denatured by heating for 3 min at 80 °C on a heat block. Spreads were then allowed to hybridize in the dark for 2 h at room temperature. Two 15-min washes were performed in a mixture containing 70% formamide, 10 mM Tris-HCl, pH 7.0, and 0.1% BSA, followed by three washes in a mixture containing 0.1 M Tris-HCl, pH 7.0, 0.15 M NaCl and 0.08% Tween-20, with DAPI added to the second wash to counter-stain the chromosomal DNA. Slides were mounted in antifade reagent (ProLong Gold, Invitrogen), and digital images were captured with a Zeiss Axioplan II microscope with a Hamamatsu C4742-95 camera using Improvise OpenLab software.

**In-gel analysis of telomeric DNA.** Pulse-field gel electrophoresis and in-gel detection of mouse telomeric DNA were performed as described previously<sup>1</sup>. Cells were resuspended in PBS and mixed 1:1 (v/v) with 2% agarose (SeaKem agarose) to obtain 5 × 10<sup>5</sup> cells per agarose plug. Plugs were digested overnight with 1 mg ml<sup>-1</sup> Proteinase K (in buffer containing 100 mM EDTA, 0.2% sodium deoxycolate, 1% sodium lauryl sarcosine), washed extensively with TE buffer (10 mM Tris-HCl, pH 8.0, 1 mM EDTA) and incubated overnight at 37 °C with 60 U MboI. The following day, the plugs were washed once in TE and once in water, and were equilibrated in 0.5 × TBE. Plugs were loaded on a 1% agarose/0.5 × TBE gel and run for 24 h using CHEF-DR1 PFG apparatus (BioRad) in 0.5 × TBE running buffer. The settings were as follows: initial pulse, 5 min; final pulse, 5 min; 6 V cm<sup>-1</sup>; 14 °C. In-gel hybridization of the native gel with <sup>32</sup>P-γATP end-labelled (CCCTAA)<sub>4</sub> oligonucleotides and subsequent denaturation and hybridization steps were performed as described<sup>30</sup>. Gels were exposed onto a PhosphorImager screen overnight, and the single-stranded G-overhang signal was quantified with ImageQuant software and normalized to the total telomeric DNA quantified after denaturation. The percentage overhang value given repre-

sents the percentage of overhang signal detectable at different time points compared to the overhang signal for the same cells not treated with Cre.

**Immunoblotting.** Cells were lysed in 2 × Laemmli buffer (100 mM Tris-HCl, pH 6.8, 200 mM DTT, 3% SDS, 20% glycerol, 0.05% bromophenol blue) at 10<sup>4</sup> cells per microliter, denatured for 7 min at 100 °C, and sheared with an insulin needle before loading the equivalent of 2 × 10<sup>5</sup> cells per lane. After immunoblotting, membranes were blocked in PBS with 5% milk and 0.1% Tween, and incubated with the following primary antibodies in 5% milk and 0.1% Tween: 53BP1 (rabbit polyclonal; 100-305, Novus Biologicals; detects endogenous mouse 53BP1, full-length wild-type and mutant human 53BP1 rescue alleles, and mCherry-BP1-2 fusion protein); MDC1 (rabbit polyclonal; 300-757, Bethyl); TRF2 (rabbit polyclonal; 647 (ref. 31)); TRF1 (1449, rabbit polyclonal; A. Sfeir and T.d.L., unpublished); CHK2 (mouse monoclonal, BD Biosciences); ATM S1981-P (mouse monoclonal; 10H11.E12, Cell Signaling); or ATM (mouse monoclonal; clone MAT3, Sigma). γ-Tubulin (mouse monoclonal, clone GTU 488, Sigma) or a non-specific band in the TRF2 western blot were used as a loading control. Blots were developed with enhanced chemiluminescence (Amersham).

**Immunofluorescence-FISH.** Cells were grown on coverslips and fixed for 10 min in 2% paraformaldehyde at room temperature followed by PBS washes (IF for γ-H2AX, MDC1 and 53BP1) or fixed for 10 min in methanol:acetone (1:1) at -20 °C followed by rehydration in PBS for 5 min (IF for NBS1). Coverslips were blocked for 30 min in blocking solution (1 mg ml<sup>-1</sup> BSA, 3% goat serum, 0.1% Triton X-100, 1 mM EDTA in PBS). Next, the cells were incubated with the following primary antibodies diluted in blocking solution for 1 h at room temperature: 53BP1 (rabbit polyclonal; 100-304A, Novus Biologicals); γ-H2AX-S139-P (mouse monoclonal; Upstate Biotechnology); MDC1 (mouse monoclonal, a gift from J. Chen); and NBS1 (rabbit polyclonal, a gift from J. Petrini). After PBS washes, coverslips were incubated with Rhodamine-Red-X-labelled secondary antibody raised against mouse or rabbit (RRX, Jackson ImmunoResearch) for 30 min and washed in PBS. At this point, coverslips were fixed with 2% paraformaldehyde for 10 min at room temperature, washed extensively in PBS, dehydrated consecutively in 70%, 95% and 100% ethanol for 5 min each, and allowed to dry completely. Hybridizing solution (70% formamide, 1 mg ml<sup>-1</sup> blocking reagent (Roche), 10 mM Tris-HCl, pH 7.2, containing PNA probe FITC-OO-(AATCCC)<sub>3</sub> (Applied Biosystems)) was added to each coverslip and the cells were denatured by heating for 10 min at 80 °C on a heat block. After 2 h incubation at room temperature in the dark, cells were washed twice with washing solution (70% formamide, 10 mM Tris-HCl, pH 7.2) and twice in PBS. DNA was counterstained with DAPI and slides were mounted in antifade reagent (ProLong Gold, Invitrogen). Digital images were captured with a Zeiss Axioplan II microscope with a Hamamatsu C4742-95 camera using Improvise OpenLab software.

To detect expression and localization of fluorescently marked proteins, cells were fixed for 10 min in 2% paraformaldehyde at room temperature. Digital images of fluorescent eGFP and mCherry signals were captured as described previously.

**Live-cell imaging.** *TRF2<sup>fl/fl</sup>*-*53BP1<sup>+/-</sup>* and *TRF2<sup>fl/fl</sup>*-*53BP1<sup>-/-</sup>* cells expressing eGFP-TRF1 (to visualize telomeres) and mCherry-BP1-2 (human 53BP1, amino acids 1220–1711, to mark dysfunctional telomeres), or *TRF2<sup>fl/fl</sup>*-*53BP1<sup>+/-</sup>*, *TRF2<sup>fl/fl</sup>*-*53BP1<sup>-/-</sup>*, *TRF2<sup>fl/fl</sup>*-*Lig4<sup>-/-</sup>*-*p53<sup>-/-</sup>* (ref. 1) and *TRF2<sup>fl/fl</sup>*-*Atm<sup>-/-</sup>* (ref. 4) cells expressing eGFP-TRF1 only, untreated or treated with Cre, were seeded onto MatTek glass bottom plates and grown for 2 days before imaging. Imaging was performed 72–84 h after Cre-mediated deletion of TRF2. Right before imaging, cells were changed into Leibovitz's L-15 medium (Gibco) supplemented with 30% FBS and allowed to equilibrate for 30 min. During the imaging session, the temperature was maintained at 37 °C with an environmental chamber. Cells were monitored using a DeltaVision RT microscope system (Applied Precision) with a PlanApo ×60 1.40 n.a. objective lens (Olympus America, Inc.). 5-μm Z-stacks at 0.5-μm steps in both eGFP and mCherry channels were acquired using SoftWoRx software with 50 ms and 30 ms exposure time, respectively, every 30 s over 20 min (*t* = 40 frames) at 2 × 2 binning with 512 × 512 pixels in final size. Images were deconvolved and projected in two dimensions using SoftWoRx software.

The tracking analysis of eGFP-TRF1-marked telomeres was performed with ImageJ software for at least ten cells for each genotype. Cells were registered by StackReg plugin using both 'Translation' and 'Scaled rotation' options. Next, particles were tracked using Particle Detector and Tracker plugin<sup>32</sup> with the following parameters for particle detection and tracking: radius = 2 pixels; cut-off = 2 pixels; percentile = 1; link range = 1; displacement = 5 pixels. The *x* and *y* coordinates of each trajectory were output for further calculation.

For each cell, 5 telomeres were chosen for analysis based on two criteria: first, they were continuously tracked for at least 35 out of 40 frames and, second, they co-localized with the mCherry-BP1-2 dysfunctional telomere marker for the

entire imaging session (20 min). To correct for cell mobility, the average  $x$  and  $y$  values of the 5 telomeres were calculated in each frame and this was used as a reference point. All data output in pixels (standard ImageJ output) were converted to metres by the formula 1 pixel = 0.2156  $\mu\text{m}$  based on the characteristics of the objective.

The following formulas were used to calculate the distance travelled between two time points, cumulative distance travelled and average speed of an individual telomere T ( $x_T^{t=n}, y_T^{t=n}$ ) relative to the reference point R ( $x_R^{t=n}, y_R^{t=n}$ ): displacement,  $D_p$ , between two time points  $t = n - 1$  and  $t = n$  (measured in  $\mu\text{m}$ ) is

$$D_n = \text{sqrt}(((x_T^{t=n} - x_R^{t=n}) - (x_T^{t=n-1} - x_R^{t=n-1}))^2 + ((y_T^{t=n} - y_R^{t=n}) - (y_T^{t=n-1} - y_R^{t=n-1}))^2)$$

Cumulative distance travelled in 20 min ( $t = 40$ )  $D_{\text{cum}}$  (measured in  $\mu\text{m}$ ) is

$$D_{\text{cum}} = \text{sum}(D_1, D_2, \dots, D_{40})$$

Average speed  $S$  (measured in  $\text{nm min}^{-1}$ ) is

$$S = D_{\text{cum}}/20$$

To calculate the displacement from the starting point ( $t = 0$ ) for a given telomere T ( $x_T^{t=n}, y_T^{t=n}$ ) at  $t = n$ , the following calculation was performed based on a reference point, R, defined as above: displacement from origin  $D_{\text{ori},t}$  is

$$D_{\text{ori},t} = \text{sqrt}(((x_T^{t=n} - x_R^{t=n}) - (x_T^{t=0} - x_R^{t=0}))^2 + ((y_T^{t=n} - y_R^{t=n}) - (y_T^{t=0} - y_R^{t=0}))^2)$$

Maximum displacement from starting point,  $D_{\text{ori MAX}}$ , for a given telomere recorded during an imaging session was used as a measure of the territory that

the telomere has sampled during the imaging session and calculated as shown below:

$$D_{\text{ori MAX}} = \max(D_{\text{ori}, 1}, D_{\text{ori}, 2}, \dots, D_{\text{ori}, 40})$$

Data were collected from three independent experiments (independent Cre infections): experiment 1 ( $n = 55$ ; Fig. 3e–g), experiment 2 ( $n = 55$ ) and experiment 3 ( $n = 65$ ; Supplementary Fig. 9). It is important to note that experiment 1 and experiment 3 were done with cell lines A ( $\text{TRF2}^{\text{fl}/-}53\text{BP1}^{+/-}$ ) and B ( $\text{TRF2}^{\text{fl}/-}53\text{BP1}^{-/-}$ ), whereas experiment 2 was performed with cell lines C ( $\text{TRF2}^{\text{fl}/-}53\text{BP1}^{+/-}$ ) and D ( $\text{TRF2}^{\text{fl}/-}53\text{BP1}^{-/-}$ ). A/B and C/D were infected with eGFP–TRF1/mCherry–BP1–2 fluorescent markers independently, which might account for the minor variation in the quantitative data on telomere mobility after deprotection.

Statistical analysis was performed using Prism Software. Mann–Whitney test (also referred to as rank sum test), which compares two unpaired groups without assuming Gaussian distribution, was applied to calculate the statistical significance values.

**Treatment with drugs.** Cells were treated with the following drugs diluted in imaging medium: actin inhibitor Latrunculin A, 0.1  $\mu\text{g ml}^{-1}$ , for 1 h before imaging and HDAC inhibitor trichostatin A, 10  $\text{ng ml}^{-1}$  and 50  $\text{ng ml}^{-1}$ , for 18 h before imaging.  $\text{TRF2}^{\text{fl}/-}$  or  $\text{TRF2}^{\text{fl}/-} \text{Lig4}^{-/-} \text{p53}^{-/-}$  cells plated on imaging plates were irradiated with 1 Gy  $\gamma$ -irradiation and imaged immediately (with 10 min delay to set up the imaging) or allowed to recover for 2 h.

28. van Steensel, B., Smogorzewska, A. & de Lange, T. TRF2 protects human telomeres from end-to-end fusions. *Cell* **92**, 401–413 (1998).
29. Lansdorp, P. M. *et al.* Heterogeneity in telomere length of human chromosomes. *Hum. Mol. Genet.* **5**, 685–691 (1996).
30. Karlseder, J., Smogorzewska, A. & de Lange, T. Senescence induced by altered telomere state, not telomere loss. *Science* **295**, 2446–2449 (2002).
31. Zhu, X. D. *et al.* Cell-cycle-regulated association of RAD50/MRE11/NBS1 with TRF2 and human telomeres. *Nature Genet.* **25**, 347–352 (2000).
32. Sbalzarini, I. F. & Koumoutsakos, P. Feature point tracking and trajectory analysis for video imaging in cell biology. *J. Struct. Biol.* **151**, 182–195 (2005).